Morphometrics reveals complex and heritable apple leaf shapes

Zoë Migicovsky[1*], Mao Li[2], Daniel H. Chitwood[3] and Sean Myles[1]

[1]Department of Plant, Food and Environmental Sciences, Faculty of Agriculture, Dalhousie University, Truro, Nova Scotia, Canada

[2]Donald Danforth Plant Science Center, St. Louis, MO, USA

[3]Independent researcher, Santa Rosa, CA, USA

*Corresponding author: Zoë Migicovsky zoe.migicovsky@dal.ca

Abstract

Apple (*Malus spp.*) is a widely grown and valuable fruit crop. Leaf shape and size are important for flowering in apple and may also be early indicators for other agriculturally valuable traits. We examined 9,000 leaves from 869 unique apple accessions using linear measurements and comprehensive morphometric techniques. We identified allometric variation in the length-to-width aspect ratio between accessions and species of apple. The allometric variation was due to variation in the width of the leaf blade, not length. Aspect ratio was highly correlated with the primary axis of morphometric variation (PC1) quantified using elliptical Fourier descriptors (EFDs) and persistent homology (PH). While the primary source of variation was aspect ratio, subsequent PCs corresponded to complex shape variation not captured by linear measurements. After linking the morphometric information with over 122,000 genome-wide SNPs, we found high narrow-sense heritability values even at later PCs, indicating that comprehensive morphometrics can capture complex, heritable phenotypes. Thus, techniques such as EFDs and PH are capturing heritable biological variation that would be missed using linear measurements

alone, and which could potentially be used to select for a hidden phenotype only detectable using comprehensive morphometrics.

Introduction

Apples (*Malus spp.*) are one of the world's most widely grown fruit crops, with the third highest global production quantity of over 84 million tonnes in 2014 (1). The shape and size of apple leaves plays an essential role in the growth and development of the tree, and ultimately impact characteristics of the fruit. Apple leaves are generally simple, with an elliptical-to-ovate shape. Previous studies in apple used linear measurements, such as length and width, to quantify leaf shape (2, 3). The length-to-width aspect ratio is a major source of variation in leaf shape. Differing aspect ratios lead to a disproportionate increase or decrease in length relative to width, or allometric variation, in leaves (4, 5). While linear measurements such as leaf length and width are useful, they fail to capture the full extent of leaf shape diversity. Failing to measure leaf shape comprehensively also limits our ability to discern the total underlying genetic contributions.

Elliptical Fourier descriptors (EFDs) are a valuable, well-recognized tool for quantifying the outline of a shape. EFD analysis first converts a contour to a chaincode, a lossless data compression method that encodes shape by a chain of numbers, in which each number indicates step-by-step movements to reconstruct the pixels comprising the shape. A Fourier decomposition is subsequently applied to the chain code, quantifying the shape as a harmonic series. EFDs have been used extensively to quantify leaf shape in diverse species, such as grape (6), tomato (7), and

47 *Passiflora* (8). Previous work used EFDs to assess apple fruit shape (9), but this technique has
48 not yet been applied to apple leaves. A newly developed morphometric technique, persistent
49 homology (PH), provides another method for estimating leaf shape. PH, like EFDs, is
50 normalized to differences in size, but it also could be orientation invariant. PH treats the pixels of
51 a contour as a 2D point cloud before applying a neighbor density estimator to each pixel. A
52 series of annulus kernels of increasing radii are used to isolate and smooth the contour densities.
53 The number of connected components is recorded as a function of density for each annulus,
54 resulting in a curve (a reduced version of persistent barcode) that quantifies shape as topology.
55 The topology-based PH approach can also be applied to serrations and root architecture, allowing
56 the similar framework to be used across different plant structures (10, 11).
57
58 Comprehensively measuring leaf shape, using approaches such as EFDs and PH, is important, as
59 shape features may be associated with agriculturally important traits. Leaves are present during
60 the lengthy juvenile phase in apple but fruits appear only on mature trees and thus, leaf traits can
61 enable early selection without the need for genetic markers. In apple, it generally takes 5 years
62 for significant fruiting to occur and any ability to discard trees not possessing a trait of interest
63 earlier in development is extremely valuable (12). There are already several cases of unique leaf
64 characteristics providing an early marker for other genetic differences in apple. For example, the
65 gene underlying red fruit flesh color may lead to anthocyanin accumulation in the leaves, causing
66 red foliage (13, 14) while columnar tree architecture may be accompanied by an increase in leaf
67 number, area, weight per unit area and length-to-width ratio (15). Leaf pH has also been
68 proposed as an early indicator of low acid fruit (16).
69

In addition to serving as early markers for other traits, leaf shape and size may influence the amount of light a tree receives, and light exposure is crucial for flowering in apple. Light penetration results in higher levels of flowering, while leaf injury or defoliation can reduce flowering (17). Thinning apple trees to a particular leaf-to-fruit ratio is a common practice to attain optimal fruit color and size. Contrastingly, trees with fewer fruit may increase vegetative growth and thus leaf area (18). In previous work, several leaf traits such as area and perimeter were correlated with apple fruit size (19). Clearly, there is an important relationship between the leaves and the fruit, and comprehensively quantifying the variation in leaf shape is a crucial component to understanding this relationship in apple.

Leaves are the main photosynthetic organs of apple, but the genetic basis underlying their shape and size remains unknown. In cotton, a single locus controls the major leaf shapes (20), but in most instances leaf shape appears to be controlled by numerous small-effect loci (5, 21). There are limited examples of genomic analyses of leaf shape in apple, however, a previous bi-parental linkage mapping study found two suggestive quantitative trait loci for leaf size (2). Previous work also measured several leaf traits such as area, perimeter and circularity, in 158 apple accessions. The study linked these measurements with 901 single nucleotide polymorphisms (SNPs) but found no significant genotype-phenotype relationships (19). Thus far, efforts have not been made to estimate the genetic heritability of comprehensive morphometric leaf phenotypes, such as those described using EFDs and PH. It therefore remains unclear to what extent these methods are capturing biologically meaningful, heritable variation.

To fully understand the genetic basis of leaf shape, it is essential to include both linear and morphometric estimates of shape. Decreasing sequencing costs and access to a large and diverse germplasm collection allowed us to analyze approximately 9,000 leaves from over 800 unique accessions which we linked to over 122,000 genome-wide SNPs. We present the first comprehensive analysis of leaf shape in apple, revealing that both accessions and species show allometric variation due to differences in the width of the leaf blade. While the primary axis of variation in apple using EFDs and PH is due to this allometric variation, we find high narrow-sense heritability values even at later principal components, indicating that comprehensive estimates of shape capture heritable variation which would be missed by linear estimates alone.

Results

Variation in apple leaf shape

We examined 24 phenotypes related to apple leaf shape and size including length, width, surface area, dry weight, leaf mass per area, within-tree variance, and overall shape estimated using PCs derived from EFD (elliptical Fourier descriptor) and PH (persistent homology) data (see Materials and Methods and Figure 1-2). The sample size and distribution of each phenotype, as well as the raw data, are provided (Figure S1; Table S1).

To visualize the primary axes of morphometric variation, we chose a representative leaf from accessions with the minimum and maximum values along the first 5 PCs for EFDs and PH (Figure 3a). The accessions with extreme values along PC1 for both methods are similar. In fact, ‘Binet Rouge’ has the lowest value along PC1 for EFD and PH, with the axis clearly

115 representing a decrease in the length-to-width (aspect) ratio. The annulus kernels most strongly
116 contributing to PH PC1 (Figure S2) provide further evidence that this PC captures variation in
117 aspect ratio. Variation in leaf shape captured by higher-order PCs is more complex and cryptic,
118 and is thus not captured using linear measurements alone. In addition, while the primary axis of
119 variation (PC1) using EFDs and PH may explain similar aspects of leaf morphology, the
120 morphospaces resulting from the two techniques differ (Figure 3b).
121
122 **Figure 3. Examples of leaf shape across PCs derived from EFDs and PH.** Binary images of
123 leaves from accessions with minimum and maximum values along PCs 1 to 5 for EFD and PH
124 estimates. PCs were calculated using values estimated as the average across 8-10 leaves but only
125 a single representative leaf is displayed. PCs were REML-adjusted based on tree position in the
126 orchard. The accession name is also listed (a). Visualization of PC1 vs PC2 for EFD and PH
127 data. Accession with minimum and maximum values along PC1 and PC2 are indicated (b).
128
129 Next, we examined the correlation between all measured traits (Table S3). By assessing the
130 correlation of PCs resulting from a classical morphometric technique such as EFDs with a novel,
131 topology-based morphometric approach like PH, we reveal how complementary the methods are
132 (Figure 4; Figure S3). While there is a highly significant correlation between PC1 for both
133 methods ($R^2 = 0.949$, $p < 1 \times 10^{-15}$), later PCs are often not significantly correlated, with the most
134 notable exception being EFD PC2 and PH PC3 ($R^2 = 0.432$, $p < 1 \times 10^{-15}$), although several other
135 PCs also show weak correlations. Thus, while the primary axis of variation (PC1) is consistent
136 and highly correlated between methods, each method captures distinct aspects of leaf
137 morphology in subsequent PCs.

Figure 4. Correlations among leaf phenotypes. Values above the diagonal are colored according to the Pearson's correlation coefficient, and those below the diagonal indicate Bonferroni-corrected p-values. The box enclosed by the dotted lines include comparisons only between phenotypes captured by comprehensive morphometric analyses.

Many of the leaf phenotypes show a strong correlation with each other (Figure 4). In particular, aspect ratio is highly correlated with PH PC1 ($r = -0.878$, $p < 1 \times 10^{-15}$), EFD PC1 ($r = -0.855$, $p < 1 \times 10^{-15}$) and minor axis (leaf blade width) ($r = -0.734$, $p < 1 \times 10^{-15}$). The correlation between the minor axis of a leaf and surface area ($r = 0.939$, $p < 1 \times 10^{-15}$) is higher than the correlation between the major axis (blade length) and surface area ($r = 0.810$, $p < 1 \times 10^{-15}$). As expected, leaf surface area is also highly correlated with average leaf dry weight ($r = 0.934$, $p < 1 \times 10^{-15}$), indicating that larger leaves are heavier.

Allometry in apple leaves

The high correlation between aspect ratio and PC1 for both EFD and PH methods indicates that length-to-width ratio is the primary source of variation in apple leaf shape. If there is an allometric relationship between the minor and major axis, and thus, the length and width of a leaf do not increase at equal rates, a slope significantly differing from 1 is expected. We find that the slope between the two measurements is significantly greater than 1 (95% CI = 1.506-1.678, $R^2 = 0.343$, $p < 1 \times 10^{-15}$), indicating that the minor axis increases at a greater rate than the major axis. While there is no significant correlation between the major axis (blade length) and EFD PC1 (R^2

= 0.001, p = 1) or PH PC1 (R^2 = 0.002, p =1), there is a significant correlation for the minor axis (blade width) and EFD PC1 (R^2 = 0.541, $p < 1 \times 10^{-15}$) and PH PC1 (R^2 = 0.573, $p < 1 \times 10^{-15}$) (Figure 5). As PC1 explains 80.23% of the variation in the leaf shape for EFDs, and 62.20% for PH, it is apparent that the width of the leaf blade, and not length, is the major source of leaf shape variation in apple. In fact, the aspect ratio, calculated as the ratio of major axis to minor axis, is even more strongly correlated with EFD and PH PC1, with an R^2 of 0.732 for EFD PC1 ($p < 1 \times 10^{-15}$) and R^2 of 0.771 for PH PC1 ($p < 1 \times 10^{-15}$). Given the significant correlation between EFD PC1 and PH PC1 (Table S3), it is not surprising that aspect ratio is highly correlated with both.

Figure 5. Correlation between the primary axis of variation (PC1) captured using EFD and PH values and leaf shape measures. The EFD PC1 is plotted against the major axis (length of leaf blade) (a), minor axis (width of leaf blade) (b) and aspect ratio (ratio of length-to-width of blade) (c). The PH PC1 is plotted against the same measures in panels d-f. The percent variances explained by PC1, prior to REML-adjustment, is shown in parentheses. All p-values are Bonferonni-corrected based on the number of comparisons in Figure 4. A regression line from a linear model with a shaded 95% confidence interval is also shown.

In addition to variation between accessions, we investigated differences in leaf shape and size between species by comparing *Malus domestica*, the domesticated apple, with its primary progenitor species, *Malus sieversii* (Table S4). PCA of the genome-wide SNP data reveals a primary axis of genetic variation that separates *M. domestica* and *M. sieversii*, although separation is incomplete (Figure 6a). The major axis (p = 0.975) of the leaves does not differ

between species (Figure 6b). However, the minor axis ($p = 4 \times 10^{-4}$) of *M. domestica* leaves are significantly larger than *M. sieversii* (Figure 6c) and the aspect ratio ($p = 0.023$) is significantly less (Figure 6d). Thus, there is allometric variation both within (Figure 5) and between (Figure 6) *Malus* species.

Figure 6. Genetic and phenotypic comparison of the domesticated apple and its wild ancestor. PCs 1 and 2 were derived from 75,973 genome-wide SNPs and samples are labeled as *M. domestica* (purple), *M. sieversii* (green) or unknown (gray). *M. domestica* leaves do not differ from *M. sieversii* leaves along the major axis (b), but they have a larger minor axis (c) and aspect ratio (d). P-values reported are Bonferroni-corrected based on multiple comparisons (Table S4). Species labels are based on USDA classification.

The genetic basis of leaf shape in apple

GWAS of the 24 leaf phenotypes examined in this study yielded few significant results. We identified 70 significant SNPs representing 5 phenotypes which are reported in Table S5. We examined the regions surrounding significant SNPs for candidate genes using the GBrowse tool (Table S6) (22). We searched within a +/- 5,000 bp window, which should capture any linked causal variation given the rapid LD decay observed in a diverse collection of apples that is largely replicated in the germplasm studied here (23). However, no strong candidate genes were identified.

While GWAS examines the genome for single, large-effect loci, genomic prediction estimates our ability to predict a phenotype using genome-wide marker data. We complimented our GWAS with genomic prediction and observed prediction accuracies (r) ranging from -0.10 to 0.52 (Table S7; Figure S5a). Aspect ratio is the primary source of variation in leaf shape (Fig 5c) and it is also the leaf measurement that had the highest genomic prediction accuracy (0.52). Other phenotypes highly correlated with aspect ratio, such as leaf width (0.51), minor axis (0.49), EFD PC1 (0.48) and PH PC1 (0.47), all had relatively high prediction accuracies. PH PC3 (0.51) was also among the most well-predicted using genetic data.

Similarly, estimates of narrow-sense heritability (h^2) calculated using GCTA (24) ranged from 0 to 0.75, with the highest heritability observed for aspect ratio (0.75) followed by leaf width (0.71), EFD PC1 (0.71), minor axis (0.69) and PH PC1 (0.65) (Figure 7; Table S8). Heritability estimates were highly correlated with genomic prediction accuracies (Figure S5b, $R^2 = 0.936$, $p < 1 \times 10^{-15}$), which is not surprising given that both techniques involve predicting a phenotype from genome-wide SNP data. None of the phenotypes measuring variance within the 8-10 leaves sampled had heritability estimates significantly different from 0.

Figure 7. Narrow-sense heritability (h^2) of leaf phenotypes. Values represent the additive genetic variance (V_g) divided by the phenotypic variance (V_p) with a standard error as calculated using GCTA (24). The dotted red lines are found at $h^2 = 0$, indicating that none of the phenotypic variance is explained by the genetic data. The proportion of the total phenotypic variance explained by each PC is indicated in parentheses.

While the principal component of variation in leaf shape detected by EFDs and PH is aspect ratio, we were also interested in determining if higher-order PCs, which capture variation not readily visible to the eye, are extracting information that is biologically meaningful. Using genomic prediction and heritability estimates, we found evidence of a genetic basis for these "hidden phenotypes", which are unmeasurable using linear techniques. For example, the heritability of phenotypes such as PH PC6 (0.48), PH PC9 (0.35), PH PC10 (0.33) and EFD PC9 (0.33) are similar to traditionally measured phenotypes such as leaf length (0.44) and leaf mass per area (0.40). While higher PCs may have relatively high heritability values, after a certain point the values (+/- standard error) overlap with 0, indicating that they are not heritable. The cutoff for morphometric PCs with a heritable genetic basis is approximately PC17. These results suggest that by making use of morphometric techniques that measure shape comprehensively, we are describing biologically meaningful, heritable phenotypes which would be missed by simple measurements such as leaf length, width and surface area.

Discussion

Leaf shape and size play a crucial role in the growth and development of apple trees, including the fruit. To elucidate the genetic basis of this variation, we quantified leaf shape in apple using traditional linear measurements and comprehensive morphometric techniques. Our work offers the first comparison between the novel topology-based technique, PH, and EFDs, which we find are complementary but distinct methods. For both methods, PC1 was highly correlated with the aspect ratio, thus providing evidence that the primary axis of variation in apple leaf shape can be captured using linear measurements. The minor axis, or width of the leaf blade, was also highly

252 correlated with PC1, while the major axis was not. Thus, variation in the aspect ratio is due to
253 variation in the leaf blade width, not length. Leaf surface area was also more highly correlated
254 with the minor axis than the major axis. Variation in leaf width is therefore essential to both the
255 size and shape of apple leaves, similar to previous work in tomato (25).
256
257 The width of the leaf blade is not only the source of variation between apple accessions, but also
258 between *M. domestica* and *M. sieversii*. The presence of the same allometric relationship within
259 and between species suggests that the genetic loci controlling intra-specific leaf shape variation
260 within *M. domestica* may be the same as those controlling the divergence in leaf shape observed
261 between the domesticated apple and its wild ancestor. For example, in birds, while PC1 and PC2
262 of bill shape explain the majority of variation across 2,000 species, they are also consistently
263 associated with the variation between higher taxa (possessing >20 species) (26). Our results
264 suggest that the increase in leaf size since domestication has not been an overall increase in leaf
265 size but specifically an increase in blade width leading to larger leaves with a reduced length-to-
266 width ratio.
267
268 Our work provides evidence that allometry is the primary source of morphometric variation in
269 apple leaves. These findings are consistent with work reported in other species such as tomato,
270 where the length-to-width ratio was the major source of shape variation (>40%) (5). Similarly,
271 work in *Passiflora* and *Vitis* species performed using two independent morphometric techniques
272 identified allometric variation as the primary source of variation in PC1, which explained at least
273 40% of the variation in leaf shape (8, 27). Thus, linear measurements—in particular aspect
274 ratio—are an important source of information when describing leaf shape. However, linear

measurements are not sufficient for capturing the full spectrum of diversity. In our study, PC1 accounts for 62.20% or 80.23% of the variation, depending on the technique used. By simply quantifying apple leaves using linear measurements, we would miss nearly 40% of the variation in some cases. While PC1 is highly correlated with aspect ratio, later PCs represent orthogonal variation that can likely only be captured through morphometric techniques such as EFDs and PH. To fully quantify variation in leaf shape, comprehensive morphometric techniques are therefore essential.

To discern the genetic contributions to leaf shape, we paired both linear and comprehensive morphometric estimates of shape with genome-wide SNP data. There are examples of a simple genetic basis of leaf shape, such as in *Arabidopsis thaliana*, where the *ANGUSTIFOLIA* and *ROTUNDIFOLIA3* independently control leaf width and length (28). In barley, transcript levels of *BFL1* limit leaf width, with overexpression resulting in narrower leaves and loss of *BFL1* function resulting in a reduced length-to-width ratio (29). Using GWAS, we found no robust associations with shape phenotypes, observed a low ratio of significant SNPs to the number of phenotypes examined, and found that significant SNPs were sparsely distributed across multiple chromosomes. In addition, the small number of significant SNPs are likely spurious associations due to poor correction for cryptic relatedness, as evidenced by the QQ plots (Fig S4). These observations suggest that leaf shape is likely polygenic and controlled by a large number of small effect loci, such as in tomato and maize (5, 21). In comparison, GWAS on apple fruit phenotypes, such as color and firmness, have revealed strong associations resulting from a small number of large effect loci (23). However, it is possible that large effect loci were missed in the present study, either because of poor reference genome assembly or inadequate marker density.

298 Improvements in genome assembly and increases in marker number will aid to further reveal the
299 genetic architecture of apple leaf shape variation.
300
301 Lastly, we investigated the degree to which leaf shape is heritable and can be predicted using
302 genome-wide SNP data. We find that the genomic prediction accuracies of the primary axes of
303 leaf shape variation are similar to previously reported estimates for fruit width (0.48) and length
304 (0.47), indicating that leaf shape is as heritable as fruit shape (23). In combination with few
305 significant GWAS results, high narrow-sense heritability estimates support a polygenic basis for
306 leaf shape. Aspect ratio was identified as the primary source of variation in leaf shape in apple
307 and had the highest genomic prediction and heritability estimates, indicating that there is a
308 genetic, heritable basis for allometric variation in apple. While we did not detect a genetic basis
309 for leaf shape variation within an accession, we intentionally sampled leaves representing the
310 mean of a tree, and this may have diminished power. Further, although the first 5 PCs for both
311 EFDs and PH explain the majority of the variation in apple leaf shape, most PCs from 1 to 14
312 have heritability estimates above 0.20 and may still represent crucial differences in leaf shape
313 from an ecological, evolutionary, or agricultural perspective. Thus, while our ability to detect the
314 primary axes of variation in leaf shape using genome-wide data is expected, our observation that
315 higher level PCs are also heritable confirms that these comprehensive morphometric methods
316 capture biologically meaningful variation that would be missed by linear measurements alone.
317
318 **Conclusions**
319

320 It is clear from our work that variation in apple leaf shape and size are under genetic control.
321 Further, high genomic prediction and heritability estimates for higher morphometric PCs indicate
322 that techniques such as EFDs and PH are capturing heritable biological variation that will be
323 missed if researchers restrict leaf shape estimates to linear measurements. Based on these results,
324 it may be possible to perform genomic selection for a phenotype that could only be detected
325 using morphometrics. If a higher order PC was correlated with a trait that was difficult or
326 expensive to measure, assessing leaf shape could potentially be used as proxy for that phenotype,
327 in the same manner that red leaf color can be used to select for red fruit flesh color in apples (13,
328 14). Additionally, a better understanding of the variation in leaf shape and size in apple could
329 ultimately have important implications for canopy management, where light exposure is crucial
330 to flowering (17). Ultimately, through the first in-depth study of leaf shape in apple, we uncover
331 allometry between accessions and species, as well as evidence that complex and heritable
332 phenotypes can be captured using comprehensive morphometric techniques.
333
334 **Materials and Methods**
335
336 *Sample collection*
337
338 Apple trees in Kentville, Nova Scotia, Canada were budded onto M.9 rootstocks in spring 2012.
339 In the fall, the trees were uprooted and kept in cold storage until spring 2013, when trees were
340 planted in an incomplete block design (see "REstricted Maximum Likelihood (REML)" below).
341 Leaves from over 900 trees were collected from August 24th to September 16th 2015. Ten leaves
342 were collected from each tree. Leaves were flattened and placed to avoid touching, then scanned

using Canon CanoScan (LiDE 220) Colour Image Scanners. Leaves were then dried for 48 hours at 65 °C and weighed to estimate the total dry weight (g) for each tree.

Morphometric analyses

Leaf scans were converted into a separate binary image for each leaf using custom ImageJ macros, which included the 'make binary' function (30). A new image file was created for each leaf and named after the tree ID. Images were converted to RGB .bmp files and a chain code analysis was performed using SHAPE (31). The chain code was used to calculate normalized elliptical Fourier descriptors (EFDs) in SHAPE. The normalized EFDs were read into Momocs v1.1.5 (32) in R (33) where harmonics B and C were removed to eliminate asymmetrical variation in leaf shape.

The binary leaf images were also analyzed using persistent homology (PH) (10). To numerically estimate the shape of the leaves using PH, we extracted the leaf contour using a 2D point cloud (Figure 1a). After centering and normalizing the contour to its centroid size, we used a Gaussian density estimator (Figure 1b), which assigns high values (red) to pixels with many neighboring pixels, and low values (blue) to pixels with fewer neighboring pixels. We multiplied the density estimator by an annulus kernel, or ring (Figure 1c), which emphasizes the shape in an annulus at the centroid and is thus invariant to orientation (Figure 1d). The resulting function can also be visualized from the side view (Figure 1e,f). As we moved a plane from top to the bottom, we recorded the number of connected components above the plane, forming a curve. With each new component this value increased, and each time components were merged, it decreased (Fig 1g).

366 For each leaf, we computed 16 curves corresponding to 16 expanding rings. For computational
367 purposes, each curve is divided into 500 numbers, ultimately resulting in the shape of each leaf
368 being represented by 8,000 (16*500) values.
369

370 **Figure 1. Visualization of persistent homology technique for annulus kernel 7.** Binary
371 images were converted into a 2D point cloud (a) which was then normalized using a Gaussian
372 density estimator (b). For each leaf, 16 annulus kernels were used. Annulus kernel 7, indicated in
373 purple (c) is used as an example for this visualization. The density estimator is multiplied by ring
374 7 (d). The function can also be visualized from the side view (e, f). As a plane moves from top to
375 bottom, the number of connected components is recorded along the curve (g). Below (g) are five
376 visualizations of curves that are represented as red vertical dotted lines in (g).
377

378 Only leaves for which both EFDs and PH shape estimations were successfully calculated were
379 included in subsequent analyses. Additionally, only trees with 8-10 leaves were included, as
380 leaves were sometimes removed due to tears, folding, or the absence of a petiole which did not
381 allow for accurate quantification of shape. The final dataset consisted of 915 trees with 8-10
382 leaves, which included 869 unique accessions and 8,995 leaves.
383

384 EFDs and PH values were averaged across leaves from an individual tree. The contribution of
385 EFD harmonics 1 to 15 to the mean leaf shape across all trees was visualized using the 'hcontrib'
386 function in the Momocs R package (Figure 2). To allow for discrimination between accessions
387 based on leaf shape, principal component analysis (PCA) was performed using the Momocs
388 'PCA' function (32) for EFDs, and the 'prcomp' function in R for PH values, which center but

389 do not scale the data. The resulting PC values were adjusted using REstricted Maximum
390 Likelihood (see below). Subsequently, we identified the accession with the minimum and
391 maximum value along each of the first 5 PCs.
392
393 **Figure 2. Contribution of elliptical Fourier descriptor harmonics to leaf shape**. The leaf
394 shapes depicted are the mean leaf shapes based on all 915 trees. Harmonics 1 to 15 are
395 represented on the x-axis and each harmonic is multiplied by the amplification factor on the y-
396 axis to visualize their contribution to mean leaf shape. An amplification factor of 0 indicates the
397 removal of the harmonic; a factor of 1 results in the normal shape; and values above 1 exaggerate
398 effects to better visualize the harmonic's contribution to the final shape.
399
400 In addition to estimating the contour of the leaf using EFDs and PH, we used several more
401 metrics to describe the leaves. Using ImageJ, we automated the measurement of leaf surface area
402 (cm^2), length (cm) of the leaf and width (cm) of the leaf as well as major (blade length) and
403 minor (blade width) axes of the best fitting ellipse—which excluded the petiole—through batch
404 processes (30). Throughout the manuscript, we use 'major' when referring to the length of the
405 leaf blade, and 'minor' when referencing the width of the leaf blade. We also calculated the
406 aspect ratio of the leaf, by dividing the major axis by the minor axis. Additionally, leaf mass per
407 area was calculated for 780 trees where we possessed surface area data for all 10 leaves, by
408 calculating the ratio of dry weight to surface area (g/cm^2).
409
410 While linear phenotypes were calculated as an average value for a particular tree, we also
411 estimated variance within a tree for aspect ratio, length, width, major and minor axis, and surface

area. Variance was calculated as the coefficient of variation using the 'cv' function in the raster package (34) in R to estimate within-tree variability in leaf size, which is indicated as 'var' throughout this manuscript.

REstricted Maximum Likelihood (REML) adjustment of phenotype data

The orchard sampled in this study is an incomplete block design with 1 of 3 standards per grid. The standards, or "control trees"—'Honeycrisp', 'SweeTango', and 'Ambrosia'—are replicated across the grid. Leaves from these trees were sampled multiple times across the orchard, which allowed us to correct for positional effects. Each phenotype was adjusted using a REstricted Maximum Likelihood (REML) model which resulted in one adjusted value per accession, even when multiple trees were measured. The impact of row grid (rGrid), column grid (cGrid) and rGrid x cGrid effects were adjusted for using the following REML model:

$$phenotype \sim accession + (1 \mid rGrid) + (1 \mid cGrid) + (1 \mid cGrid{:}rGrid)$$

We fit a linear mixed-effects model via REML using the 'lmer' function in the lme4 package in R (35) and then calculated the least squares means using the 'lsmeans' function in the lsmeans R package (36).

Thus, while the initial phenotype data was collected for 915 trees, following REML adjustment, one value remained per unique accession, resulting in 869 accessions. REML-adjustment was applied directly to all size, weight and variance estimates. For PH and EFDs, we applied the

434 REML following PCA and thus the percent contribution for each PC was calculated using
435 unadjusted values. The adjusted data for all 24 phenotypes are included in Table S1.
436
437 *Phenomic analyses*
438
439 The correlation between leaf phenotypes was calculated using Pearson's correlation and p-values
440 were Bonferroni-corrected for multiple comparisons. The resulting heatmap was visualized using
441 the 'geom_tile' function in ggplot2 in R (37). Next, we examined the leaves for allometry using
442 the 'SMA' function in the smartr R package (38) to estimate if the slope between the log-
443 transformed minor and major axis differed from 1.
444
445 Accessions were labelled as either *Malus* x. *domestica* Borkh. or *Malus sieversii* Lebed. based on
446 information provided by the United States Department of Agriculture (USDA) Germplasm
447 Resources Information Network website (http://www.ars-grin.gov/) (Table S2). We used a
448 Mann-Whitney U test to test if any phenotypes differed between species and Bonferroni-
449 corrected all p-values for multiple comparisons.
450
451 *Genomic analyses*
452
453 DNA was extracted using commercial extraction kits. Genotyping-by-sequencing (GBS) libraries
454 were prepared using ApeKI and PstI-EcoT221I restriction enzymes according to Elshire, *et al.*
455 (39). GBS libraries were sequenced using Illumina Hi-Seq 2000 technology. Reads which failed
456 Illumina's "chastity filter" were removed from raw fastq files. Remaining reads were aligned to

457 the *Malus* x. *domestica* v1.0 pseudo haplotype reference sequence (40) using the Burrows-
458 Wheeler aligner tool v0.7.12 (41) and the Tassel version 5 pipeline (42). Tassel parameters
459 included a minKmerL of 30, mnQS of 20, mxKmerNum of 50000000 and batchSize of 20. The
460 kmerlength was set to 82 for ApeKI and 89 for PstI-EcoT22I based on the max barcode size. The
461 minMAF for the DiscoverySNPCallerPluginV2 was set to 0.01. All other default parameters
462 were used. Non-biallelic sites and indels were removed using VCFtools v.0.1.14 (43). VCFs for
463 both enzymes were then merged using a custom perl script, preferentially keeping SNPs called
464 by PstI-EcoT22I at overlapping sites, since those sites tended to be at higher coverage.
465
466 Missing data was imputed using LinkImputeR v0.9 (Money et al., Submitted, available:
467 http://www.cultivatingdiversity.org/software.html) with global thresholds of 0.01 for minor allele
468 frequency (MAF) and 0.70 for missingness. We examined depths of 3 to 8 and selected a case
469 for imputation with a max position/sample missingness of 0.70, a minimum depth of 5, and an
470 imputation accuracy of 94.9%. The VCF was converted to a genotype table using PLINK v1.07
471 (44, 45).
472
473 Of the 869 accessions assessed in this study, 816 had genomic data following imputation and
474 filtering and were included in downstream analyses. The resulting genotype table consisted of
475 816 accessions and 197,565 SNPs. Subsequently, a 0.05 MAF filter was applied using PLINK,
476 after which 128,132 SNPs remained. SNPs with more than 90% heterozygous genotypes were
477 removed. The final genotype table consisted of 816 samples and 122,596 SNPs.
478

479 To perform PCA, SNPs were pruned for linkage disequilibrium (LD) using PLINK. We
480 considered a window of 10 SNPs, removing one SNP from a pair if $R^2 > 0.5$, then shifting the
481 window by 3 SNPs and repeating (PLINK command: indep-pairwise 10 3 0.5). This resulted in a
482 set of 75,973 SNPs for 816 accessions. PCA was performed on the LD-pruned genome-wide
483 SNPs using 'prcomp' in R with data that were centered but not scaled. The first 2 genomic PCs
484 were visualized using ggplot2 in R (37).
485
486 We performed a genome-wide association study (GWAS) using the mixed linear model in Tassel
487 (version 5) for each phenotype, adjusting for relatedness among individuals using a kinship
488 matrix as well as the first 3 PCs for population structure (46, 47). The threshold for significance
489 was calculated using simpleM (48, 49) which estimates the number of PCs needed to explain
490 0.995 of the variance, or the number of independent SNPs. The inferred Meff used to calculate
491 the significance threshold was 91,667 SNPs.
492
493 We searched the regions surrounding any significant GWAS SNPs using the Genome Database
494 for Rosaceae GBrowse tool for *Malus* x. *domestica* v1.0 p genome (22). We used a window of
495 +/- 5,000 bp (10 kb) surrounding the significant SNP to check for genes, and when identified, we
496 used the basic local alignment search tool (BLAST) from NCBI to search for the mRNA
497 sequence and reported the result with the max score (50).
498
499 Genomic prediction was performed using the 'x.val' function in the R package PopVar (51). The
500 rrBLUP model was selected and 5-fold (nFold=5) cross-validation was repeated 3 times
501 (nFold.reps=3) with no further filtering (min.maf=0) from the set of 122,596 SNPs used for

GWAS. All other default parameters were used. In addition to performing genomic prediction on the main 24 phenotypes examined in this study, we performed genomic prediction on all 40 PCs for EFDs and on the first 40 PCs for PH values. We also used the 'rnorm' function in R to generate 1,000 random phenotypes with a mean of 0 and a standard deviation of 1, and performed genomic prediction using these random phenotypes to obtain the range of genomic prediction accuracies one can expect at random. Lastly, we used genome-wide complex trait analysis (GCTA) v.1.26.0 which estimates the genetic relationships between individuals based on genome-wide SNPs and uses this information to calculate the variance explained by these SNPs. The ratio of additive genetic variation to phenotypic variance is used to calculate narrow-sense heritability (h^2), or SNP heritability, of a trait (24). We used GCTA to estimate heritability for each phenotype, including the first 40 PCs for EFD and PH. We also estimated the correlation between genomic prediction accuracy (r) and narrow-sense heritability (h^2) using a Pearson's correlation.

Acknowledgments

This article was written, in part, thanks to funding from the Canada Research Chairs program, the National Sciences and Engineering Research Council of Canada and Genome Canada. Z.M. was also supported in part by a Killam Predoctoral Scholarship from Dalhousie University. We would like to acknowledge Gavin Douglas and Sherry Fillmore for their help setting up the statistical design of the orchard and SNP-calling pipeline. We also thank all past and present members of the Myles Lab for their work in maintaining the apple orchard.

525 **Supplementary Material**

526 **Figure S1. Distribution of leaf phenotypes following REML-adjustment.** N is equal to the
527 total number of unique samples.

528 **Figure S2. Visualization of contributions of each ring to PH PC1.** Rings 6, 7 and 16
529 contribute the most to leaf shape according to PH PC1. The placement of each ring is visualized
530 on a leaf representing the minimum and maximum value along PC1 (a). The contribution to PC1
531 of each of the 16 rings is also shown (b).

532

533 **Figure S3. Comparison of morphometric EFD and PH PCs 1 to 5.** Correlation between first 5
534 PCs, estimated using Pearson's correlation, including R^2 and Bonferroni corrected p-values
535 based on Figure 4/Table S3.

536

537 **Figure S4. GWAS results for all 24 leaf phenotypes examined.** Manhattan and QQ plots are
538 included for each phenotype. The QQ-plot shows both the results of a naive GWAS (Pearson
539 correlation) and the results from applying the mixed model. P-values are log-transformed and the
540 threshold for significance is simpleM-corrected and indicated by a horizontal dotted line.
541 Chromosome R indicates SNPs found on contigs unanchored to the reference genome.

542

543 **Figure S5. Genomic prediction accuracy (r) (a) and correlation between genomic prediction**
544 **results and narrow-sense heritability estimates (h^2) for all leaf phenotypes (b).** Genomic
545 prediction accuracies represent the average correlation (+/- standard deviation) between observed
546 and predicted phenotype scores, based on 5-fold cross-validation with 3 iterations. Dotted red
547 lines indicate the minimum and maximum prediction average accuracy (r) achieved using 1,000

548 randomly generated phenotypes. The percent variance explained by each PC was calculated prior
549 to REML-adjustment and is indicated in parentheses.
550
551 **Table S1. All leaf phenotypes assessed in apple, following REML-adjustment.** Accessions
552 are identified by their unique "apple id". Further information about these accessions is available
553 in Table S2.
554
555 **Table S2. Metadata for all accessions assessed in this study.** In addition to the unique numeric
556 apple_id, we report the Germplasm Origin (where budwood was obtained from) and Species
557 (*Malus domestica*/*Malus sieversii*).
558
559 **Table S3. Correlation between leaf phenotypes as well as Bonferroni-adjusted p-values.**
560 Pearson's product moment correlation coefficients are reported. These results are visualized in
561 Figure 2.
562
563 **Table S4. Comparison of leaf phenotypes between accessions based on metadata.**
564 Bonferroni-adjusted p-values resulting from a Mann-Whitney U test estimating the difference
565 between accessions based on species (*Malus domestica*/*Malus sieversii*) for the leaf phenotypes
566 examined.
567
568 **Table S5. Positional information for significant GWAS results.** Additional information about
569 significant SNPs are included such as p-value, marker R^2, minor and major allele, minor and
570 major effect and MAF.

Table S6. Genes found within +/- 5 kb of SNPs with significant associations to phenotypes from GWAS. Results are listed according to the Genome Database for Rosaceae GBrowse (accessed January 27 2017). Overlapping mRNA, length, contig, GO category, GO term accession, GO term name, InterPro Term, InterPro Description and NCBI sequence with Max Score when BLASTed using NCBI are reported.

Table S7. Genomic prediction accuracies (r) for leaf phenotypes. r_avg represents the average correlation between observed and predicted phenotype scores, based on 5-fold cross-validation with 3 iterations. The standard deviation (r_sd) is also reported.

Table S8. Narrow-sense heritability (h^2) for leaf phenotypes. h^2 represents the genetic variance (V_g) divided by the phenotypic variance (V_p). The standard error (SE) is also reported. These results are visualized in Figure 7.

References

1. Food and Agriculture Organization of the United Nations (2017) FAOSTAT.
2. Liebhard R, Kellerhals M, Pfammatter W, Jertmini M, & Gessler C (2003) Mapping quantitative physiological traits in apple (Malus × domestica Borkh.). *Plant Molecular Biology*:511–526.
3. Bassett CL, Glenn DM, Forsline PL, Wisniewski ME, & Farrell RE (2011) Characterizing Water Use Efficiency and Water Deficit Responses in Apple (Malus× domestica Borkh. and Malus sieversii Ledeb.) M. Roem. *HortScience* 46(8):1079-1084.
4. Gurevitch J (1992) Sources of Variation in Leaf Shape among Two Populations of Achillea Lanulosa. *Genetics* 130(2):385-394.
5. Chitwood DH, *et al.* (2013) A quantitative genetic basis for leaf morphology in a set of precisely defined tomato introgression lines. *The Plant cell* 25(7):2465-2481.

6. Chitwood DH, *et al.* (2014) A modern ampelography: a genetic basis for leaf shape and venation patterning in grape. *Plant physiology* 164(1):259-272.
7. Chitwood DH, *et al.* (2012) The developmental trajectory of leaflet morphology in wild tomato species. *Plant physiology* 158(3):1230-1240.
8. Chitwood DH & Otoni WC (2017) Morphometric analysis of Passiflora leaves: the relationship between landmarks of the vasculature and elliptical Fourier descriptors of the blade. *GigaScience* 6(1):1-13.
9. Currie AJ, *et al.* (2000) Quantitative evaluation of apple (Malus × domestica Borkh.) fruit shape by principal component analysis of Fourier descriptors. *Euphytica* 111(3):219–227.
10. Li M, *et al.* (2017) Persistent homology: a tool to universally measure plant morphologies across organs and scales. *bioRxiv*.
11. Li M, Duncan K, Topp CN, & Chitwood DH (2017) Persistent homology and the branching topologies of plants. *American journal of botany* 104(3):349-353.
12. Kumar S, Bink MCAM, Volz RK, Bus VGM, & Chagné D (2012) Towards genomic selection in apple (Malus × domestica Borkh.) breeding programmes: Prospects, challenges and strategies. *Tree Genetics & Genomes* 8(1):1-14.
13. Espley RV, *et al.* (2009) Multiple repeats of a promoter segment causes transcription factor autoregulation in red apples. *The Plant cell* 21(1):168-183.
14. Chagne D, *et al.* (2007) Mapping a candidate gene (MdMYB10) for red flesh and foliage colour in apple. *BMC Genomics* 8:212.
15. Talwara S, Grout BWW, & Toldam-Andersen TB (2013) Modification of leaf morphology and anatomy as a consequence of columnar architecture in domestic apple (Malus×domestica Borkh.) trees. *Scientia Horticulturae* 164:310-315.
16. Visser T & Verhaegh J (1978) Inheritance and selection of some fruit characters of apple. II. The relation between leaf and fruit pH as a basis for preselection. *Euphytica* 27(3):761-765.
17. Dennis F, Jr. (2003) Flowering, Pollination and Fruit Set and Development. *Apples: Botany, Production and Uses*, eds Ferree DC & Warrington IJ (CABI Publishing), pp 153-166.
18. Wünsche JN, Palmer JW, & Greer DH (2000) Effects of Crop Load on Fruiting and Gas-exchange Characteristics of 'Braeburn'/M. 26 Apple Trees at Full Canopy. *Journal of the American Society for Horticultural Science* 125(1):93-99.
19. Khan MA, Olsen KM, Sovero V, Kushad MM, & Korban SS (2014) Fruit Quality Traits Have Played Critical Roles in Domestication of the Apple. *The Plant Genome* 7(3):0.
20. Andres RJ, *et al.* (2017) Modifications to a LATE MERISTEM IDENTITY1 gene are responsible for the major leaf shapes of Upland cotton (Gossypium hirsutum L.). *Proc Natl Acad Sci U S A* 114(1):E57-E66.
21. Tian F, *et al.* (2011) Genome-wide association study of leaf architecture in the maize nested association mapping population. *Nat Genet* 43(2):159-162.
22. Jung S, *et al.* (2014) The Genome Database for Rosaceae (GDR): year 10 update. *Nucleic Acids Res* 42(Database issue):D1237-1244.
23. Migicovsky Z, *et al.* (2016) Genome to Phenome Mapping in Apple Using Historical Data. *The Plant Genome* 9(2).
24. Yang J, Lee SH, Goddard ME, & Visscher PM (2011) GCTA: a tool for genome-wide complex trait analysis. *American journal of human genetics* 88(1):76-82.

644 25. Schwarz D & Kläring H-P (2001) Allometry to estimate leaf area of tomato. *Journal of*
645 *Plant Nutrition* 24(8):1291-1309.
646 26. Cooney CR, *et al.* (2017) Mega-evolutionary dynamics of the adaptive radiation of birds.
647 *Nature* 542(7641):344-347.
648 27. Klein LL, *et al.* (2017) Digital Morphometrics of Two North American Grapevines
649 (Vitis: Vitaceae) Quantifies Leaf Variation between Species, within Species, and among
650 Individuals. *Frontiers in Plant Science* 8(373).
651 28. Tsuge T, Tsukaya H, & Uchimiya H (1996) Two independent and polarized processes of
652 cell elongation regulate leaf blade expansion in Arabidopsis thaliana (L.) Heynh.
653 *Development* 122(5):1589-1600.
654 29. Jöst M, *et al.* (2016) The INDETERMINATE DOMAIN Protein BROAD LEAF1 Limits
655 Barley Leaf Width by Restricting Lateral Proliferation. *Current Biology* 26(7):903-909.
656 30. Abràmoff MD, Magalhães PJ, & Ram SJ (2004) Image processing with ImageJ.
657 *Biophotonics international* 11(7):36-42.
658 31. Iwata H & Ukai Y (2002) SHAPE: a computer program package for quantitative
659 evaluation of biological shapes based on elliptic Fourier descriptors. *Journal of Heredity*
660 93(5):384-385.
661 32. Bonhomme V, Picq S, Gaucherel C, & Claude J (2014) Momocs: outline analysis using
662 R. *Journal of Statistical Software* 56(13):1-24.
663 33. R Core Team (2016) R: A Language and Environment for Statistical Computing (R
664 Foundation for Statistical Computing, Vienna, Austria).
665 34. Hijmans RJ (2016) raster: Geographic Data Analysis and Modeling).
666 35. Bates D, Mächler M, Bolker B, & Walker S (2015) Fitting Linear Mixed-Effects Models
667 Using lme4. *2015* 67(1):48.
668 36. Lenth RV (2016) Least-squares means: the R package lsmeans. *J Stat Softw* 69(1):1-33.
669 37. Wickham H (2009) *ggplot2: Elegant Graphics for Data Analysis* (Springer-Verlag New
670 York).
671 38. Warton DI, Duursma RA, Falster DS, & Taskinen S (2012) smatr 3- an R package for
672 estimation and inference about allometric lines. *Methods in Ecology and Evolution*
673 3(2):257-259.
674 39. Elshire RJ, *et al.* (2011) A robust, simple genotyping-by-sequencing (GBS) approach for
675 high diversity species. *PloS one* 6(5):e19379.
676 40. Velasco R, *et al.* (2010) The genome of the domesticated apple (Malus [times] domestica
677 Borkh.). *Nat Genet* 42(10):833-839.
678 41. Li H & Durbin R (2009) Fast and accurate short read alignment with Burrows-Wheeler
679 transform. *Bioinformatics* 25(14):1754-1760.
680 42. Glaubitz JC, *et al.* (2014) TASSEL-GBS: A High Capacity Genotyping by Sequencing
681 Analysis Pipeline. *PloS one* 9(2):e90346.
682 43. Danecek P, *et al.* (2011) The variant call format and VCFtools. *Bioinformatics*
683 27(15):2156-2158.
684 44. Purcell S, *et al.* (2007) PLINK: A Tool Set for Whole-Genome Association and
685 Population-Based Linkage Analyses. *The American Journal of Human Genetics*
686 81(3):559-575.
687 45. Purcell S (2009) PLINK v.1.07.
688 46. Bradbury PJ, *et al.* (2007) TASSEL: software for association mapping of complex traits
689 in diverse samples. *Bioinformatics* 23(19):2633-2635.

690 47. Zhang Z, *et al.* (2010) Mixed linear model approach adapted for genome-wide
691 association studies. *Nature genetics* 42(4):355-360.
692 48. Gao X, Becker LC, Becker DM, Starmer JD, & Province MA (2010) Avoiding the high
693 Bonferroni penalty in genome‐wide association studies. *Genetic epidemiology*
694 34(1):100-105.
695 49. Gao X, Starmer J, & Martin ER (2008) A multiple testing correction method for genetic
696 association studies using correlated single nucleotide polymorphisms. *Genetic*
697 *epidemiology* 32(4):361-369.
698 50. Altschul SF, Gish W, Miller W, Myers EW, & Lipman DJ (1990) Basic local alignment
699 search tool. *Journal of molecular biology* 215(3):403-410.
700 51. Mohammadi M, Tiede T, & Smith KP (2015) PopVar: A Genome-Wide Procedure for
701 Predicting Genetic Variance and Correlated Response in Biparental Breeding
702 Populations. *Crop Science* 55(5):2068.
703

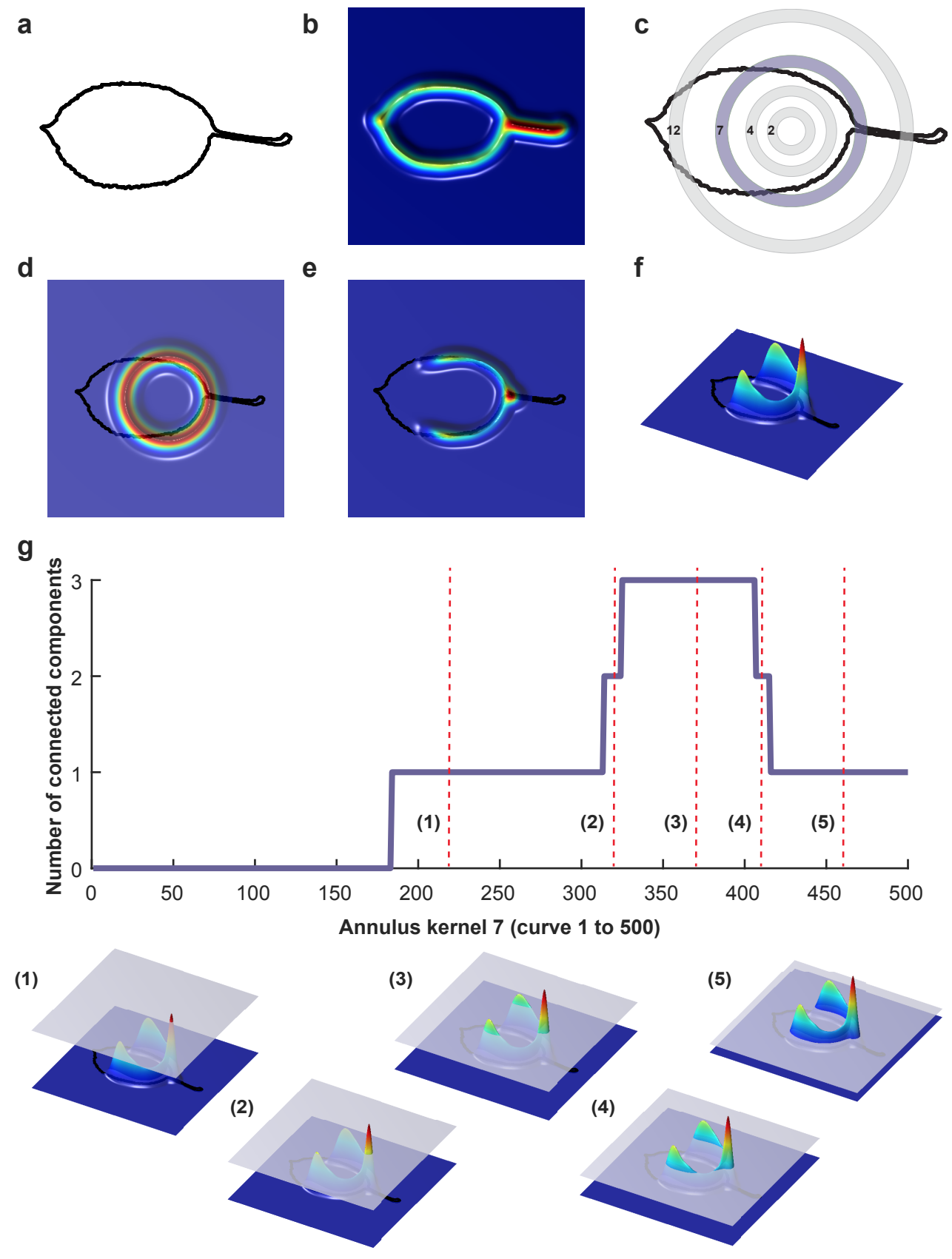
a
b
c
12
7
4
2
d
e
f
g
Number of connected components
0
1
2
3
0
50
100
150
200
250
300
350
400
450
500
Annulus kernel 7 (curve 1 to 500)
(1)
(2)
(3)
(4)
(5)
(1)
(2)
(3)
(4)
(5)

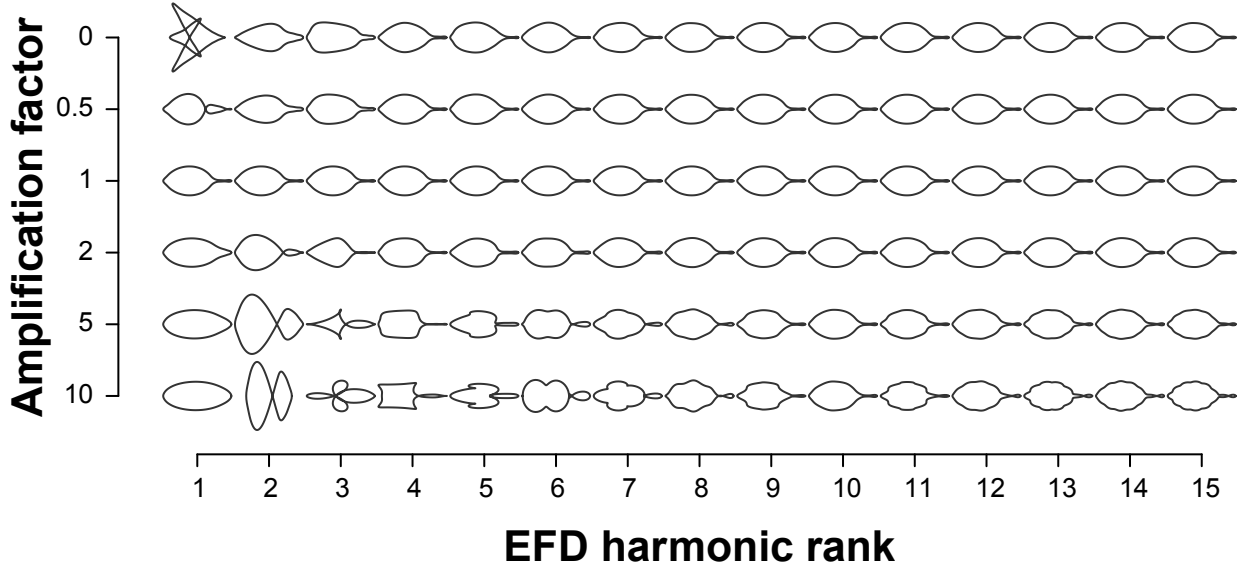
Amplification factor
0
0.5
1
2
5
10
1
2
3
4
5
6
7
8
9
10
11
12
13
14
15
EFD harmonic rank

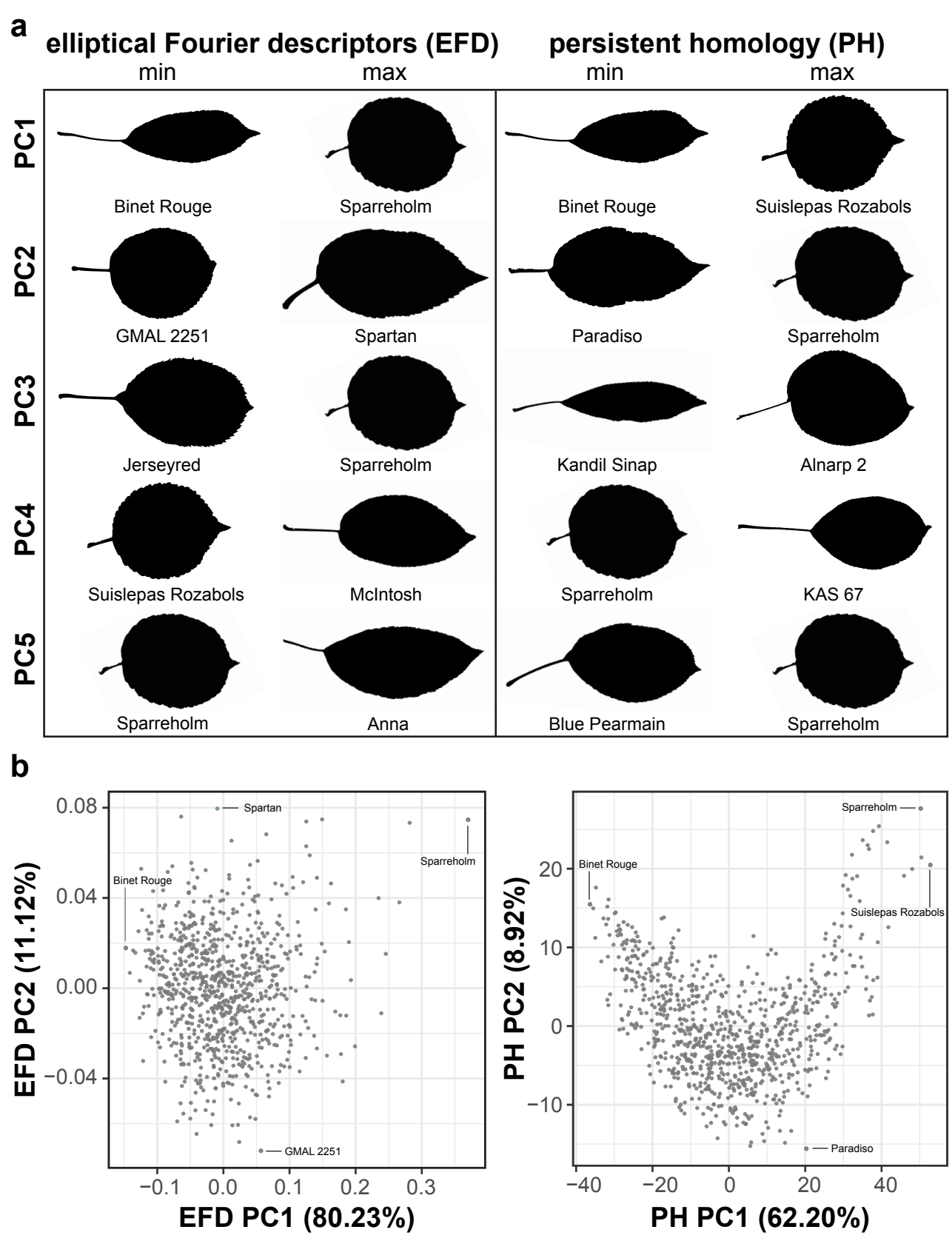
a
elliptical Fourier descriptors (EFD)
persistent homology (PH)
min
max
min
max
PC1
PC2
PC3
PC4
PC5
Binet Rouge
Sparreholm
Binet Rouge
Suislepas Rozabols
GMAL 2251
Spartan
Paradiso
Sparreholm
Jerseyred
Sparreholm
Kandil Sinap
Alnarp 2
Suislepas Rozabols
McIntosh
Sparreholm
KAS 67
Sparreholm
Anna
Blue Pearmain
Sparreholm
b
EFD PC2 (11.12%)
EFD PC1 (80.23%)
Spartan
Sparreholm
Binet Rouge
GMAL 2251
PH PC2 (8.92%)
PH PC1 (62.20%)
Sparreholm
Binet Rouge
Suislepas Rozabols
Paradiso

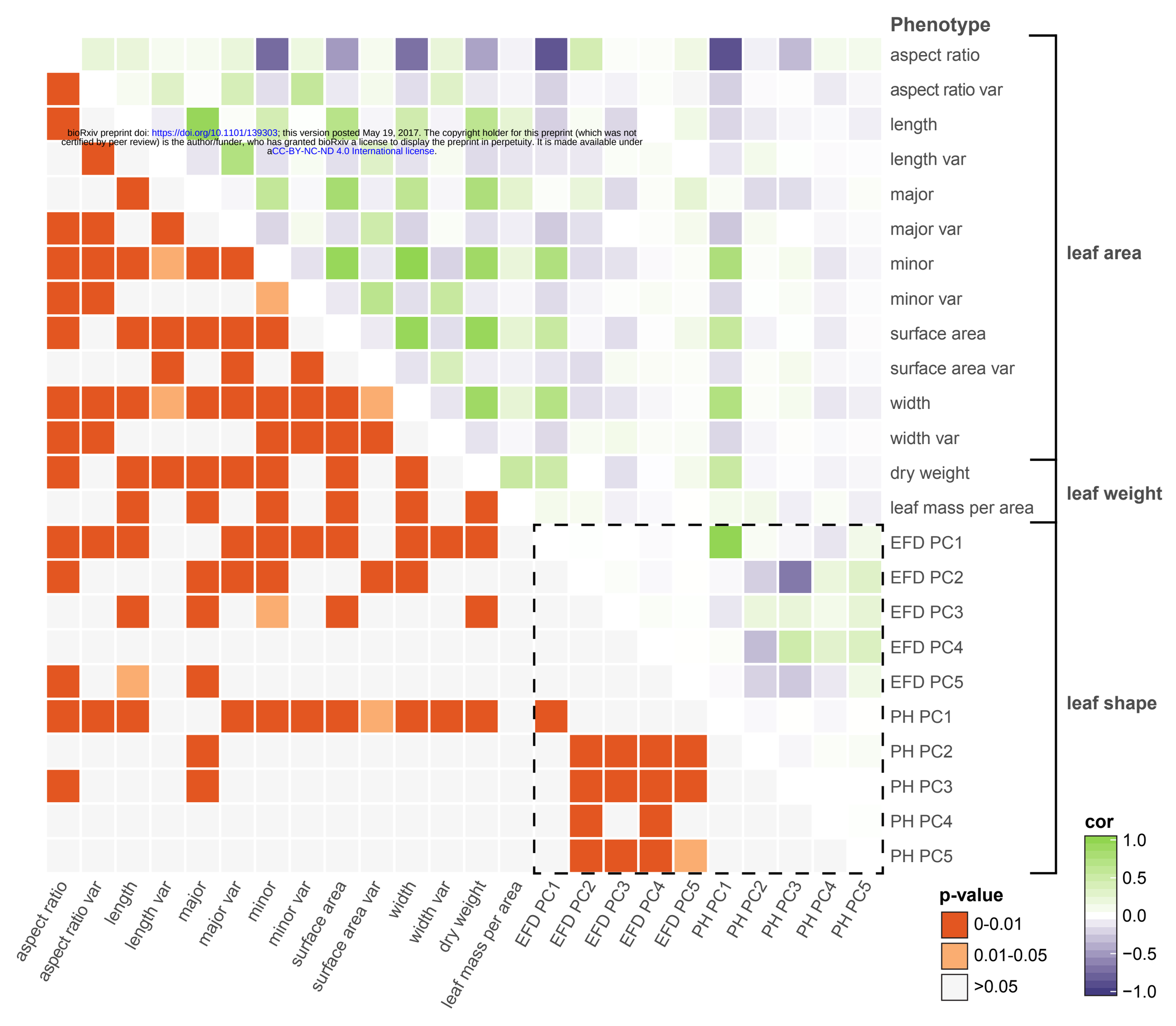

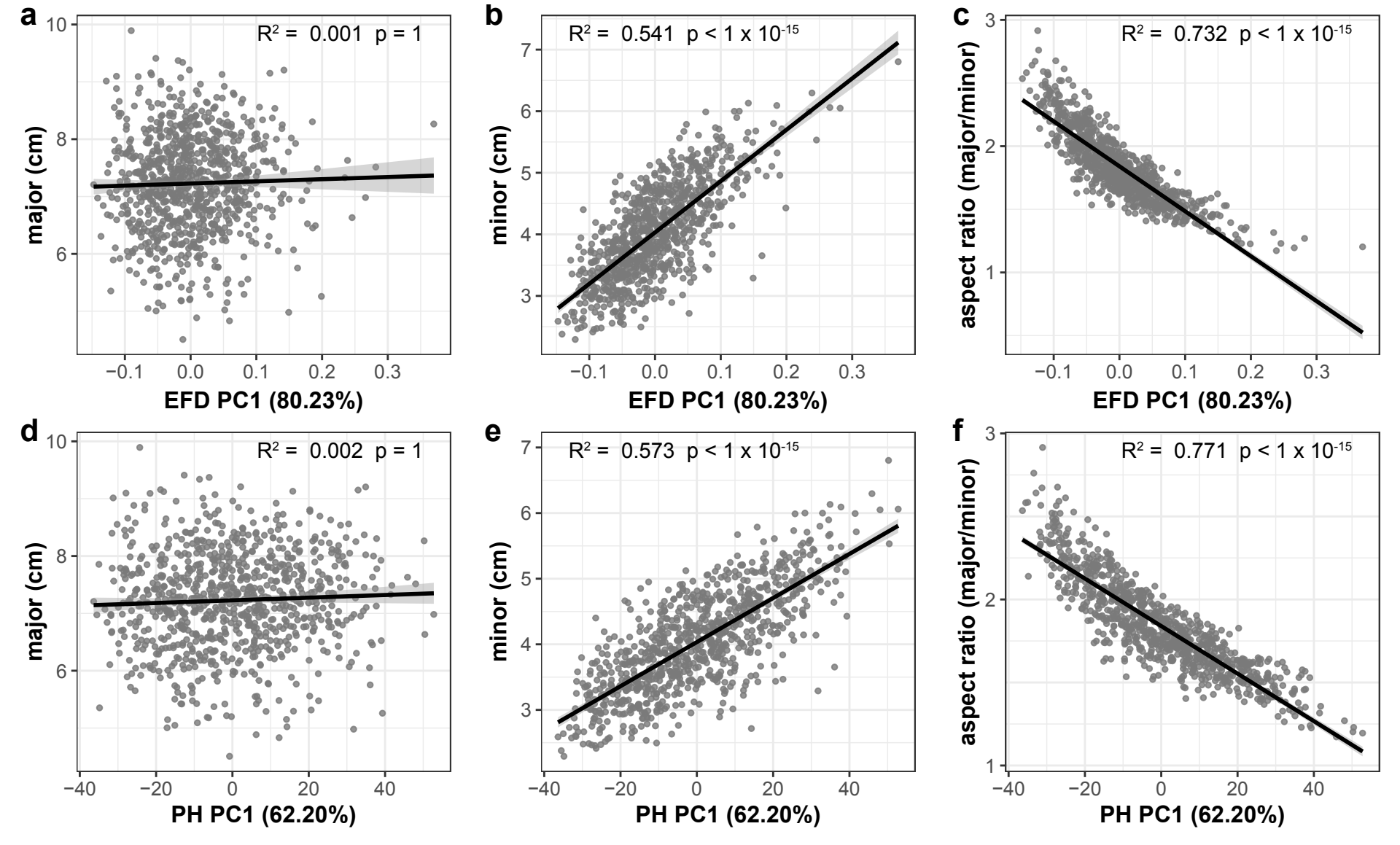
a
b
c
d
e
f
R² = 0.001 p = 1
R² = 0.541 p < 1 x 10-15
R² = 0.732 p < 1 x 10-15
R² = 0.002 p = 1
R² = 0.573 p < 1 x 10-15
R² = 0.771 p < 1 x 10-15
major (cm)
minor (cm)
aspect ratio (major/minor)
EFD PC1 (80.23%)
PH PC1 (62.20%)

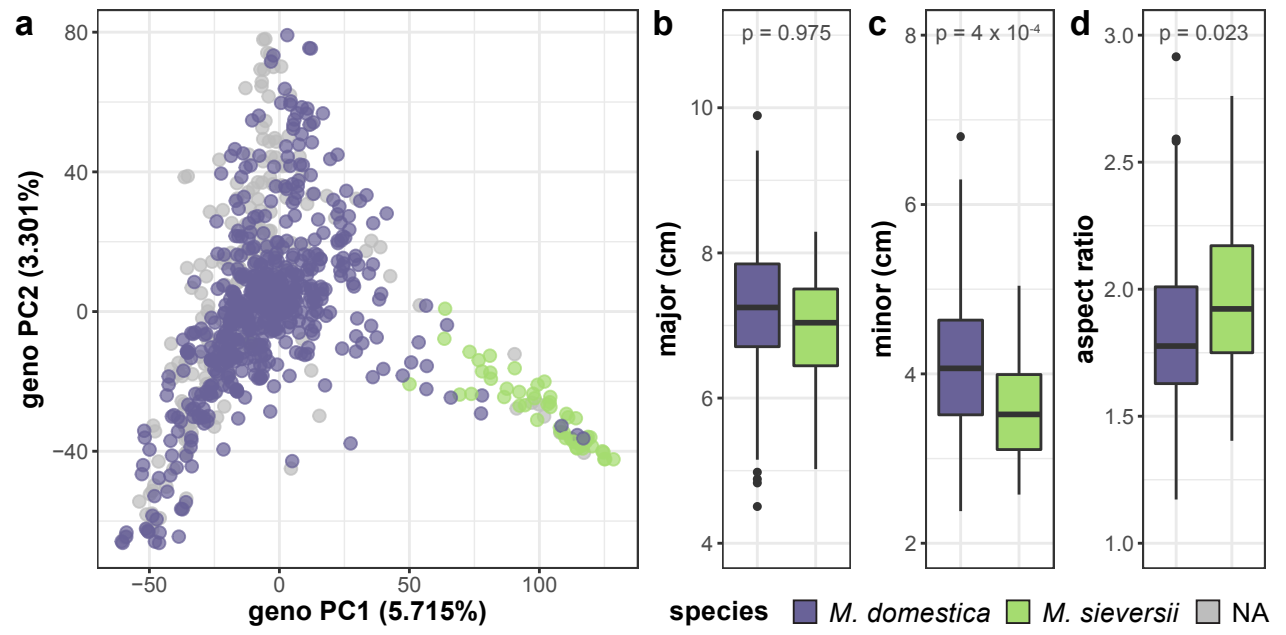
a
b
c
d
geno PC2 (3.301%)
geno PC1 (5.715%)
major (cm)
minor (cm)
aspect ratio
p = 0.975
p = 4 x 10-4
p = 0.023
species
M. domestica
M. sieversii
NA

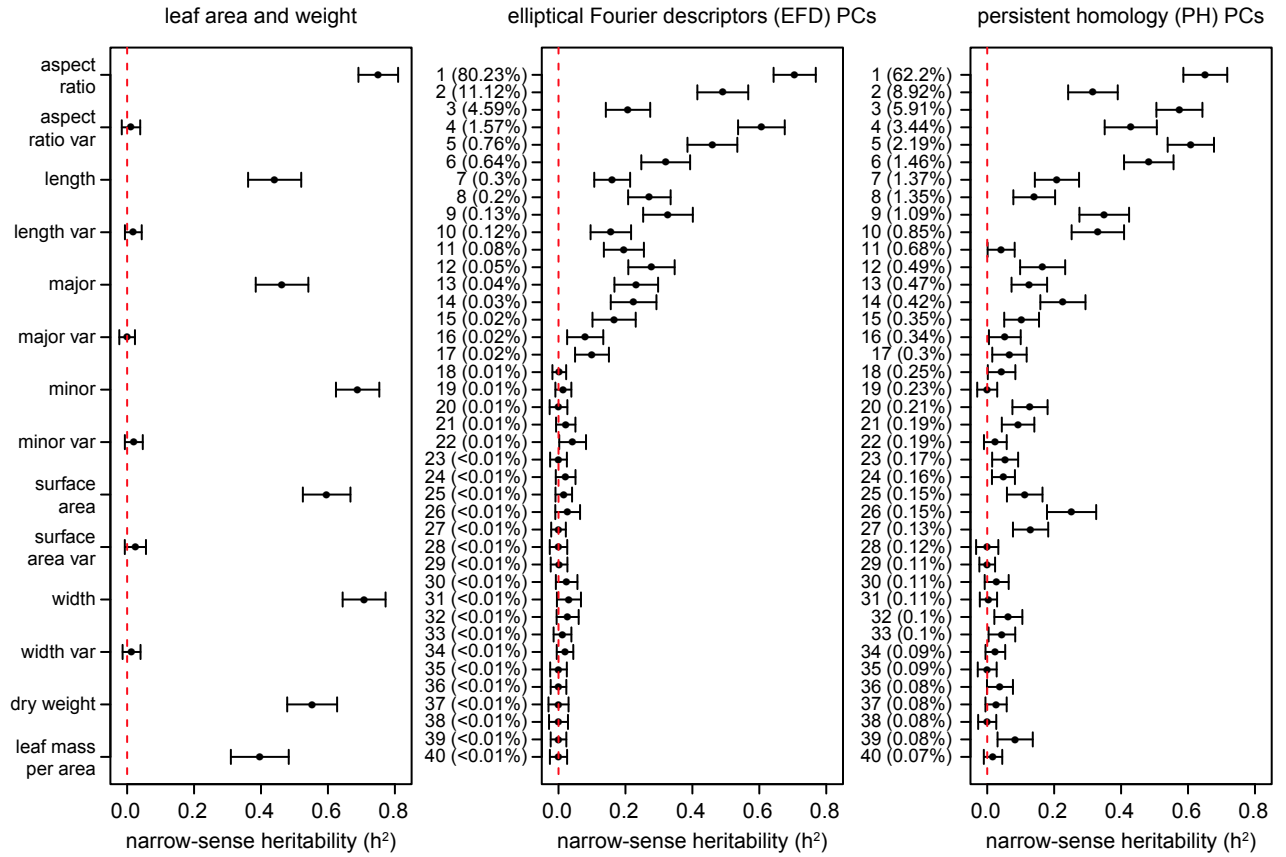
leaf area and weight
aspect ratio
aspect ratio var
length
length var
major
major var
minor
minor var
surface area
surface area var
width
width var
dry weight
leaf mass per area
0.0
0.2
0.4
0.6
0.8
narrow-sense heritability (h2)
elliptical Fourier descriptors (EFD) PCs
1 (80.23%)
2 (11.12%)
3 (4.59%)
4 (1.57%)
5 (0.76%)
6 (0.64%)
7 (0.3%)
8 (0.2%)
9 (0.13%)
10 (0.12%)
11 (0.08%)
12 (0.05%)
13 (0.04%)
14 (0.03%)
15 (0.02%)
16 (0.02%)
17 (0.02%)
18 (0.01%)
19 (0.01%)
20 (0.01%)
21 (0.01%)
22 (0.01%)
23 (<0.01%)
24 (<0.01%)
25 (<0.01%)
26 (<0.01%)
27 (<0.01%)
28 (<0.01%)
29 (<0.01%)
30 (<0.01%)
31 (<0.01%)
32 (<0.01%)
33 (<0.01%)
34 (<0.01%)
35 (<0.01%)
36 (<0.01%)
37 (<0.01%)
38 (<0.01%)
39 (<0.01%)
40 (<0.01%)
0.0
0.2
0.4
0.6
0.8
narrow-sense heritability (h2)
persistent homology (PH) PCs
1 (62.2%)
2 (8.92%)
3 (5.91%)
4 (3.44%)
5 (2.19%)
6 (1.46%)
7 (1.37%)
8 (1.35%)
9 (1.09%)
10 (0.85%)
11 (0.68%)
12 (0.49%)
13 (0.47%)
14 (0.42%)
15 (0.35%)
16 (0.34%)
17 (0.3%)
18 (0.25%)
19 (0.23%)
20 (0.21%)
21 (0.19%)
22 (0.19%)
23 (0.17%)
24 (0.16%)
25 (0.15%)
26 (0.15%)
27 (0.13%)
28 (0.12%)
29 (0.11%)
30 (0.11%)
31 (0.11%)
32 (0.1%)
33 (0.1%)
34 (0.09%)
35 (0.09%)
36 (0.08%)
37 (0.08%)
38 (0.08%)
39 (0.08%)
40 (0.07%)
0.0
0.2
0.4
0.6
0.8
narrow-sense heritability (h2)